



OPEN ACCESS

EDITED BY

Anwen Shao,
Zhejiang University, China

REVIEWED BY

Aimin Jiang,
Fudan University, China
Zhengrui Li,
Shanghai Jiao Tong University, China

*CORRESPONDENCE

Jian Gong

✉ gongjian88@tom.com

Yaohua Zhang

✉ yaohuaz@ccmu.edu.cn

Lingxuan An

✉ Lingxuan.An@med.uni-muenchen.de

RECEIVED 10 May 2023

ACCEPTED 20 July 2023

PUBLISHED 17 August 2023

CITATION

Han X, Yan Z, Fan K, Guan X, Hu B, Li X, Ou Y, Cui B, An L, Zhang Y and Gong J (2023) The combined signatures of telomere and immune cell landscape provide a prognostic and therapeutic biomarker in glioma. *Front. Immunol.* 14:1220100. doi: 10.3389/fimmu.2023.1220100

COPYRIGHT

© 2023 Han, Yan, Fan, Guan, Hu, Li, Ou, Cui, An, Zhang and Gong. This is an open-access article distributed under the terms of the [Creative Commons Attribution License \(CC BY\)](https://creativecommons.org/licenses/by/4.0/). The use, distribution or reproduction in other forums is permitted, provided the original author(s) and the copyright owner(s) are credited and that the original publication in this journal is cited, in accordance with accepted academic practice. No use, distribution or reproduction is permitted which does not comply with these terms.

The combined signatures of telomere and immune cell landscape provide a prognostic and therapeutic biomarker in glioma

Xu Han¹, Zihan Yan¹, Kaiyu Fan¹, Xueyi Guan¹, Bohan Hu¹, Xiang Li¹, Yunwei Ou¹, Bing Cui², Lingxuan An^{3*}, Yaohua Zhang^{2*} and Jian Gong^{1,4*}

¹Department of Neurosurgery, Beijing Tiantan Hospital, Capital Medical University, Beijing, China, ²Beijing Institute of Brain Disorders, Laboratory of Brain Disorders, Ministry of Science and Technology, Collaborative Innovation Center for Brain Disorders, Capital Medical University, Beijing, China,

³Department of General, Visceral, and Transplant Surgery, Ludwig-Maximilians-University Munich, Munich, Germany, ⁴Beijing Neurosurgical Institute, Capital Medical University, Beijing, China

Background: Gliomas, the most prevalent primary malignant tumors of the central nervous system in adults, exhibit slow growth in lower-grade gliomas (LGG). However, the majority of LGG cases progress to high-grade gliomas, posing challenges for prognostication. The tumor microenvironment (TME), characterized by telomere-related genes and immune cell infiltration, strongly influences glioma growth and therapeutic response. Therefore, our objective was to develop a Telomere-TME (TM-TME) classifier that integrates telomere-related genes and immune cell landscape to assess prognosis and therapeutic response in glioma.

Methods: This study encompassed LGG patients from the TCGA and CCGA databases. TM score and TME score were derived from the expression signatures of telomere-related genes and the presence of immune cells in LGG, respectively. The TM-TME classifier was established by combining TM and TME scores to effectively predict prognosis. Subsequently, we conducted Kaplan-Meier survival estimation, univariate Cox regression analysis, and receiver operating characteristic curves to validate the prognostic prediction capacity of the TM-TME classifier across multiple cohorts. Gene Ontology (GO) analysis, biological processes, and proteomaps were performed to annotate the functional aspects of each subgroup and visualize the cellular signaling pathways.

Results: The TM_{low}+TME_{high} subgroup exhibited superior prognosis and therapeutic response compared to other subgroups ($P < 0.001$). This finding could be attributed to distinct tumor somatic mutations and cancer cellular signaling pathways. GO analysis indicated that the TM_{low}+TME_{high} subgroup is associated with the neuronal system and modulation of chemical synaptic transmission. Conversely, the TM_{high}+TME_{low} subgroup showed a strong association with cell cycle and DNA metabolic processes. Furthermore, the

classifier significantly differentiated overall survival in the TCGA LGG cohort and served as an independent prognostic factor for LGG patients in both the TCGA cohort ($P < 0.001$) and the CGGA cohort ($P < 0.001$).

Conclusion: Overall, our findings underscore the significance of the TM-TME classifier in predicting prognosis and immune therapeutic response in glioma, shedding light on the complex immune landscape within each subgroup. Additionally, our results suggest the potential of integrating risk stratification with precision therapy for LGG.

KEYWORDS

telomere related genes, glioma, tumor microenvironment, prognosis, immune response

1 Introduction

Glioma, which accounts for approximately 80% of all malignant brain tumors, represents one of the most commonly observed primary brain tumors in clinical practice (1). The 2016 World Health Organization (WHO) revision classifies glioma into four grades. Grades II and III are collectively referred to as diffuse lower-grade gliomas (LGG), while grade IV is known as glioblastoma (GBM) (2). GBM is a fatal tumor with a median overall survival (OS) of merely 15 months. In contrast, patients diagnosed with WHO II and WHO III gliomas have median OS durations of 78.1 and 37.6 months, respectively (3). Despite advancements in diagnostic and therapeutic outcomes, a subset of LGG patients may experience disease progression, leading to unfavorable therapeutic responses and a worsened prognosis.

The conventional treatment modalities for LGG encompass surgical intervention, radiotherapy, and chemotherapy. However, the emergence of immunotherapy has introduced a potential revolution in clinical management and improved survival rates for LGG patients. Nonetheless, its efficacy remains limited to a small subset of individuals. Currently, predictive biomarkers utilized in clinical practice include O6-methylguanine DNA methyltransferase (MGMT) promoter methylation, 1p/19q codeletion, and isocitrate dehydrogenase (IDH) mutation, among others (4, 5). Nevertheless, the existing pool of investigated biomarkers fails to provide sufficient accuracy for prognosis prediction and optimal treatment selection.

Telomeres, the repeated TTAGGG DNA sequences located at chromosome ends, are associated with the shelterin complex (6). These specialized structures are essential for chromosome stability, and aberrations in telomeres have been implicated in numerous diseases, including various forms of cancer (7). A 2017 Mendelian randomization study analyzing 16 telomere length-related single nucleotide polymorphisms (SNPs) from 130 genome-wide association studies (GWAS) revealed that genetically longer telomeres are associated with an elevated risk of several cancers, including lung cancer, ovarian cancer, neuroblastoma, and glioma (8). The primary regulation of telomere length is attributed to the telomerase complex, comprising an RNA template and the

telomerase reverse transcriptase (TERT) enzyme (9). Notably, TERT exerts significant influence on angiogenesis, invasion, epithelial-mesenchymal transformation (EMT), inflammation, immunosuppression, and other critical gene expression profiles, even in a telomere-independent manner. These TERT-mediated activities may profoundly affect the dynamics and homeostasis of the tumor microenvironment (TME) (10–12). Several studies have validated the association between TERT promoter mutations and the prognosis of glioma patients. In particular, individuals with TERT promoter mutations demonstrated a more favorable prognosis compared to those with wildtype TERT promoter, specifically in grade II or III oligodendroglioma, 1p/19q-codeleted patients, and IDH-mutant cases (13, 14).

In the present study, we leveraged the features of telomeres and immune cells to establish Telomere (TM) and TME scores, respectively. Recognizing the telomere-mediated regulation of TME and the implications for prognosis and immunotherapy, we developed an integrated TM-TME classifier utilizing these scores to effectively predict prognosis and immunotherapy response. Remarkably, distinct patient subgroups within the LGG cohort exhibited varying prognostic outcomes, somatic mutation (SM) landscapes, responses to therapy, and enriched pathways. These findings hold promising implications for the improvement of clinical disease management.

2 Methods

2.1 Source of the data

The training set for this study comprised the mRNA expression profiles and corresponding clinical data of the TCGA LGG cohort, which were obtained from the UCSC Xena database (<https://xena.ucsc.edu/>). To validate the findings, we also acquired the mRNAseq_693 dataset from the CGGA database, serving as the confirmation set. Our analysis focused exclusively on LGG patients with WHO grades II and III, utilizing the aforementioned datasets. To visualize the TM scores within each cell, we obtained two public single-cell RNA sequencing (scRNA-seq) cohorts, namely

GSE70630 and GSE89567, from the Gene Expression Omnibus repository (GEO) (15), specifically the mRNAseq_693 data set. The analysis focused exclusively on LGG patients classified as WHO grades II and III in the aforementioned datasets. Moreover, two publicly available single-cell RNA sequencing (scRNA-seq) cohorts, namely GSE70630 and GSE89567, were retrieved from the GEO (Gene Expression Omnibus repository) to enable the visualization of TM scores at the cellular level (16, 17). Subsequently, the bulk RNA sequencing data underwent a $\log_2(\text{TPM}+1)$ transformation for further analyses.

2.2 Identification of prognostic telomere-associated genes and TME cells

We utilized the URL of <http://www.cancertelsys.org/telnet/to> obtain the genes associated with telomeres (18). In order to identify prognostic-associated telomere genes in the TCGA-LGG dataset, we performed univariate Cox regression analysis and least absolute shrinkage and selection operator (LASSO) regression analysis on 2093 telomere-associated genes using the bootstrap approach (18, 19). We utilized the URL of <http://www.cancertelsys.org/telnet/to> obtain the genes associated with telomeres (18). In order to identify prognostic-associated telomere genes in the TCGA-LGG dataset, we performed univariate Cox regression analysis and least absolute shrinkage and selection operator (lasso) regression analysis on 2093 telomere-associated genes using the bootstrap approach (20, 21). The TCGA LGG cohort incorporates the CIBERSORT algorithm, which estimates the composition of 22 immune cells in distinct tissues based on gene expression signatures for TME cells (22, 23). The TCGA LGG cohort incorporates the CIBERSORT algorithm, which estimates the composition of 22 immune cells in distinct tissues based on gene expression signatures for TME cells.

2.3 Construction of TM score, TME score, and TM-TME classifier

The establishment of the TM and TME scores was based on the 18 telomere-associated genes derived from the TCGA LGG cohort and the coefficients (Coef) of five immune cells for multivariate Cox regression analysis (24). To enhance the accuracy of both the TM and TME models, we randomly selected 1000 samples from the entire LGG sample pool and conducted multivariate Cox analysis on each sample (25). Moreover, we obtained the standard deviation (SD) values of the Coef for each gene and cell. The weights in the respective models were determined by the ratio of the Coef to the SD values. In summary, the following formula was employed to calculate the TM score:

$$TM \text{ score} = \sum_{i=1}^{18} \frac{Coef_i}{SD_i} * exp(gene_i)$$

Similarly, the TME score calculating formula is:

$$TME \text{ score} = -\sum_{j=1}^5 \frac{Coef_j}{SD_j} * fra(cell_j)$$

Where $exp(gene_i)$ denotes the gene i 's expression level and $fra(cell_j)$ denotes the cell j 's fraction. Using the median value of each dataset's TM and TME scores, the TM-TME classifier was then constructed. Samples in each cohort were divided into "TM_low+TME_high (TM_L+TME_H)", "TM_high+TME_low (TM_H+TME_L)", and "Mixed" [TM_low+TME_low (TM_L+TME_L), TM_high+TME_high (TM_H+TME_H)] groups. The "timeROC" package was utilized for assessing the prognostic prediction power of the TM-TME classifier using receiver operating characteristic (ROC) curves (26, 27).

2.4 Visualization of TM score at the single-cell level

To analyze the single-cell data, we employed Seurat objects designed for scRNA-seq gene expression matrix, enabling clustering analysis, annotation, and visualization (28, 29). Transcriptomes expressing between 200 and 7000 genes were retained. To reduce dimensionality, a principal component (PC) analysis was conducted on the top 3000 genes exhibiting the highest variability. Subsequently, t-SNE (t-distributed stochastic neighbor embedding) was applied for visualizing the single-cell data. Cell type annotations were derived using cell type markers reported in the published literature (30, 31). The aforementioned formula related to the TM model was utilized to compute the TM score for each individual cell.

In addition, we utilized The Tumor Immune Single-Cell Hub (TISCH; <http://tisch.comp-genomics.org>) (32, 33), an extensive online resource providing specific single-cell RNA-seq data related to the tumor microenvironment (TME), to systematically investigate the diverse composition of the TME across distinct datasets and cell types.

2.5 Weighted gene co-expression network analysis, enrichment analysis, and construction of the interacted network

The identification of the gene module influencing the TM-TME classifier was achieved using WGCNA (34, 35). WGCNA analysis was performed on the TCGA LGG expression profile, selecting the top 5000 genes based on their median absolute deviations. To discover potential hub genes, the key module exhibiting the strongest association with the subgroups was determined. Subsequent evaluation of hub genes within the co-expression module of highest significance was conducted using Metascape (<http://metascape.org>) (36), a gene function enrichment and categorization tool. To uncover interconnected hub genes, the MCODE algorithm was employed. Each MCODE network was assigned a distinct color to represent the close interacting associations between molecules. Additionally, a list of differentially expressed proteins was inputted into an internet tool (<https://proteomaps.net/>) to generate proteomaps (37).

2.6 SM and immunotherapy response

The mutation annotation format (MAF) data pertaining to the TCGA LGG cohort could be accessed through the TCGA database. In order to compare the SM status within different subgroups of the TM-TME classifier, we generated waterfall diagrams using the “maftools” package to illustrate the mutations in the top 20 genes (38, 39). Moreover, the tumor mutational burden (TMB) of each LGG sample was calculated by determining the total number of somatic mutations (SMs) per million bases in the tumor genome, after excluding germ-line mutations. To predict the clinical response to immune checkpoint blockade (ICB) in melanoma and other tumor patients, the TIDE web platform incorporates relevant ICB trials published in the literature (40, 41).

2.7 Total RNA extraction and quantitative real-time polymerase chain reaction

We employed quantitative real-time polymerase chain reaction (qRT-PCR) to investigate the expression patterns of 18 selected pivotal genes in both LGG tissues and their corresponding peritumoral tissues, which were obtained from a cohort of five patients who underwent surgical intervention. Total RNA was extracted using TRIZOL reagent (Life technologies, USA), followed by reverse transcription reactions performed with a qPCR RT Kit (Yeason, China). Subsequently, qRT-PCR was conducted on a LightCycler 480 SYBR Green I instrument (Roche, Mannheim, Germany) to determine the expression levels of the target genes (42). The forward and reverse primers for the 18 pivotal genes and GAPDH were provided in Supplementary Table S3. To normalize the gene expression, the expression of GAPDH was utilized as a reference, and the relative expression levels of the 18 key mRNAs were calculated using the $2^{-\Delta\Delta Ct}$ method.

2.8 Western blotting, immunohistochemical, and immunofluorescence staining

Tumor and peritumoral specimens were lysed by RIPA buffer (Solarbio, Beijing, China) supplemented with protease and phosphatase inhibitors. Subsequently, the lysates were subjected to SDS-PAGE separation and transferred onto PVDF membranes. Immunoblotting was performed using antibodies against WEE1 (CST, 13084) and β -actin (proteintech, HRP-60008).

For immunohistochemical and immunofluorescence analyses, tumor and corresponding peritumoral tissues were obtained from three patients. Paraffin-embedded tissues were sectioned and subjected to heat treatment in sodium citrate buffer. Blocking of the sections was accomplished using goat serum, followed by overnight incubation with primary antibodies at 4°C. Subsequently, a secondary antibody conjugated with horseradish peroxidase was applied, and 3'-diaminobenzidine was utilized for sample visualization. Hematoxylin was used for counterstaining, and the sections were examined under a microscope.

2.9 Statistical analysis

In the current study, version 4.1.2 of the R statistical software package was utilized for all statistical analyses. The examination of relationships between variables was conducted using both Pearson and Spearman correlation methods. To compare different subgroups, nonparametric tests including the Wilcoxon rank sum test and Kruskal-Wallis rank sum test were employed. The significance level was set at $p < 0.05$, and statistical significance was denoted by “*”, “**”, and “***” for p-values less than 0.05, 0.01, and 0.001, respectively.

3 Results

3.1 Construction of TM and TME scores

An integrated approach was employed in the TCGA LGG cohort to estimate the telomere and immune cell status of patients. Initially, univariate cox analysis, lasso regression analysis of genes related to telomere maintenance (TM genes), and KM OS estimation of immune cells were conducted (Figures 1A, B). The results of the univariate cox analysis yielded 1198 TM genes, which are documented in Supplementary Table S1. Subsequently, the TM and tumor microenvironment (TME) scores were derived, comprising 18 TM genes and five distinct immune cell types, respectively. Supplementary Table S2 presents a comprehensive overview of these scores. To assess the prognostic significance, multivariate analysis was performed separately for the 18 TM genes and the five immune cell types (Figures 2A, B). Additionally, the interplay between the 18 telomere-associated genes and the five TME cells in the TCGA LGG set was explored and visualized in Figure 2E. Furthermore, KM survival curves demonstrated that patients with low TM scores exhibited superior survival outcomes compared to those with high TM scores, whereas the opposite trend was observed for the TME score (Figures 2C, D).

3.2 Immune activate with different risk score in TM score

The tumor microenvironment plays a critical role in both tumorigenesis and the efficacy of immunotherapeutic interventions. To gain a deeper understanding, we conducted further investigations into the TME milieu of patients with low-grade glioma (LGG) who were classified into high and low risk groups based on the TM score, using the CIBERSORT algorithm. Initially, we arranged the LGG patients in ascending order according to their TM risk scores, visualizing the distribution of various immune cell types based on their respective risk scores (Figure 2F). The interrelationships among immune cells in LGG patients (Figure 2G) can provide valuable insights into the immune microenvironment specific to certain tumor types. Subsequently, we observed a higher prevalence of T cells CD4 memory resting, Monocytes, and Macrophages M2 within the immune cell composition of LGG patients, leading us to

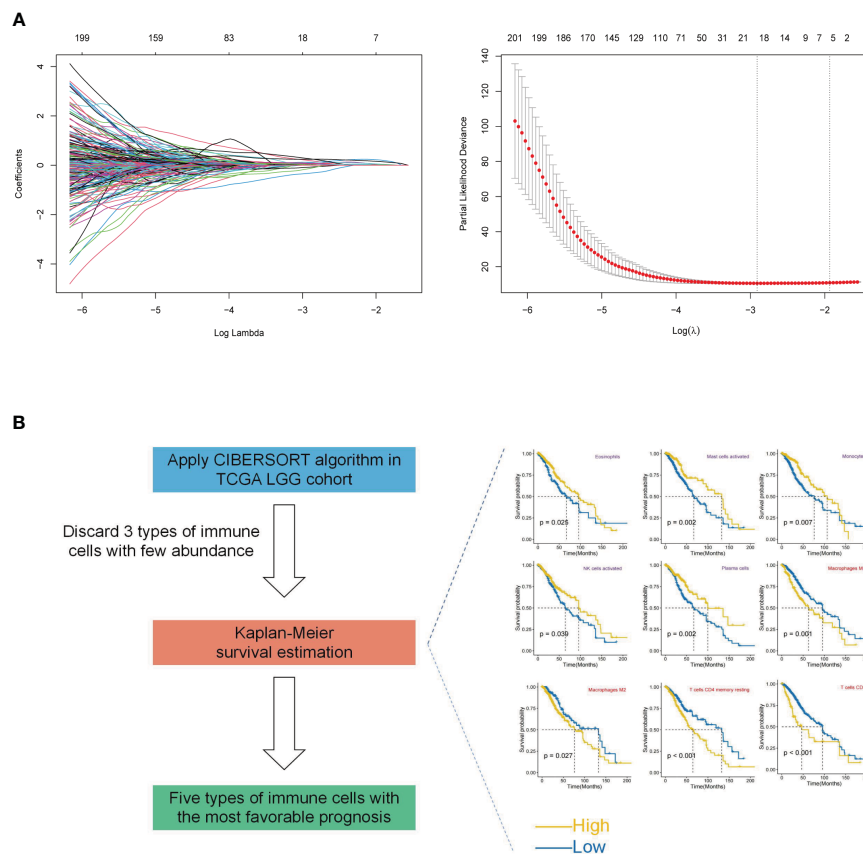


FIGURE 1

Construction of TM and TME scores. **(A)** Lasso regression analysis was performed for selected 1198 TM genes in the TCGA LGG cohort. Ultimately, the TM score was developed using 18 telomere-associated genes. **(B)** The CIBERSORT method was utilized to determine the abundance of 22 different types of immune cells in the TCGA LGG cohort. Kaplan-Meier (KM) survival curve analysis was performed for the remaining types of immune cells after excluding 3 types of immune cells with low levels. Only the types of immune cells whose p-values were < 0.05 were presented in KM overall survival curves shown on the right-hand side (favorable and unfavorable prognostic factors are respectively denoted by the colors purple and red). The TME score was determined using a combination of activated NK cells, plasma cells, monocytes, mast cells, and eosinophils.

hypothesize that these three cell types might exert influence on patients' prognoses, a supposition supported by previous investigations (Figure 2H). Notably, the infiltration of multiple immune cell populations correlates closely with the 18 selected gene signatures employed in constructing the TM score model (Figure 2I). Lastly, we employed a lollipop chart to provide a detailed representation of the associations between genes and immune cell infiltrations (Figure 3).

3.3 Single-cell analysis of LGG based on TM score

To investigate the TM score within the single-cell transcriptomic landscape of lower-grade glioma (LGG), we performed t-SNE analysis on single-cell datasets derived from two different sources (Supplementary Figures S1A, B). By assessing the elevated expression levels of gene sets corresponding to specific cell type markers, namely PTPRZ1 for tumor cells, MOBP for oligodendrocytes, and CSF1R for macrophages (Supplementary Figures S1C, D), we successfully classified the cells. Subsequently, we computed the TM scores individually for each cell type (Figures 4A–D). Notably, the

macrophages exhibited considerably higher TM scores compared to both the tumor cells and oligodendrocytes (Figures 4E, F), thus affirming a strong association between telomere and the immune cells of the tumor microenvironment (TME) at the single-cell level.

3.4 Correlation analysis of 17 telomere related genes and tumor immune microenvironment at the single-cell level

The single-cell dataset Glioma_GSE131928_10X was acquired from the TISCH database for the purpose of investigating the 17 selected genes (GATA5, which is not present in the dataset), within the TME (43). Within the GSE131928 dataset, a total of 27 cell clusters and 8 distinct cell types were identified, including malignant cells, monocytes/macrophages, oligodendrocytes, exhausted CD8+ T cells (referred to as CD8+Tex), and others. Figure 5A illustrates the distribution and abundance of the various cell types. AC-like malignant cells and CD8+Tex cells were found to predominantly express MSN, whereas MT3 exhibited predominant expression in malignant cells, AC-like malignant cells, MES-like malignant cells, OPC-like malignant cells, and oligodendrocytes,

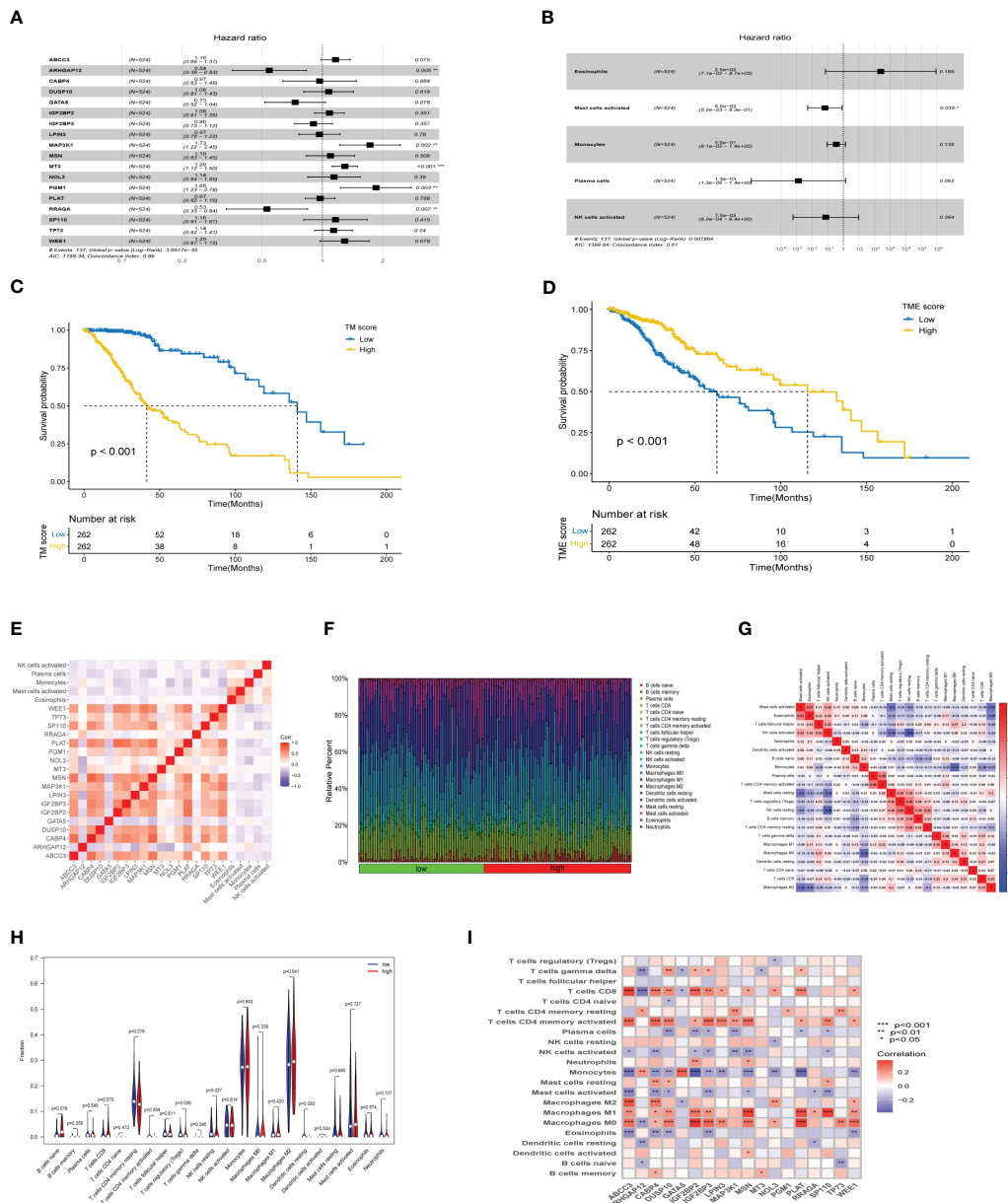


FIGURE 2 TM and TME score development and performance in LGG. (A, B) The multivariate cox regression-based forest plot showed 18 telomere-associated genes and 5 TME cells linked to overall survival (OS). (C, D) Kaplan-Meier survival curves for subgroups characterized by high and low TM and TME scores. (E) Heatmap showing the spearman correlation matrix of the telomere-associated genes and TME cells. The positive, negative, and insignificant correlations are denoted respectively by the colors red, blue, and blank. (F) The ratio of infiltrating immune cells categorized by their risk score. (G) Correlation of immune cells. (H) Differences in immune cell composition between high-risk group and low-risk group. (I) Correlation between 18 telomere related genes and immune cells. * $p < 0.05$, ** $p < 0.01$, *** $p < 0.001$.

with minimal expression observed in NPC-like malignant cells and immune cells, CD8+Tex (Figures 5B, 6).

3.5 TM-TME was an independent prognostic indicator for the LGG cohort

Based on the aforementioned findings, we developed a TM-TME classifier by utilizing the median value of TM and TME scores

for each dataset. To evaluate the prognostic prediction power of the TM-TME classifier, KM OS curves were employed. The patient cohort was categorized into four subgroups based on the TM-TME classifier: TM_L+TME_H, TM_L+TME_L, TM_H+TME_H, and TM_H+TME_L. Notably, the TM-TME classifier demonstrated statistically significant prognostic implications in the TCGA LGG cohort (Figure 7A). It was observed that the prognostic significance is heavily influenced by both TM and TME scores. In light of the marginal prognostic disparities between TM_L+TME_L and

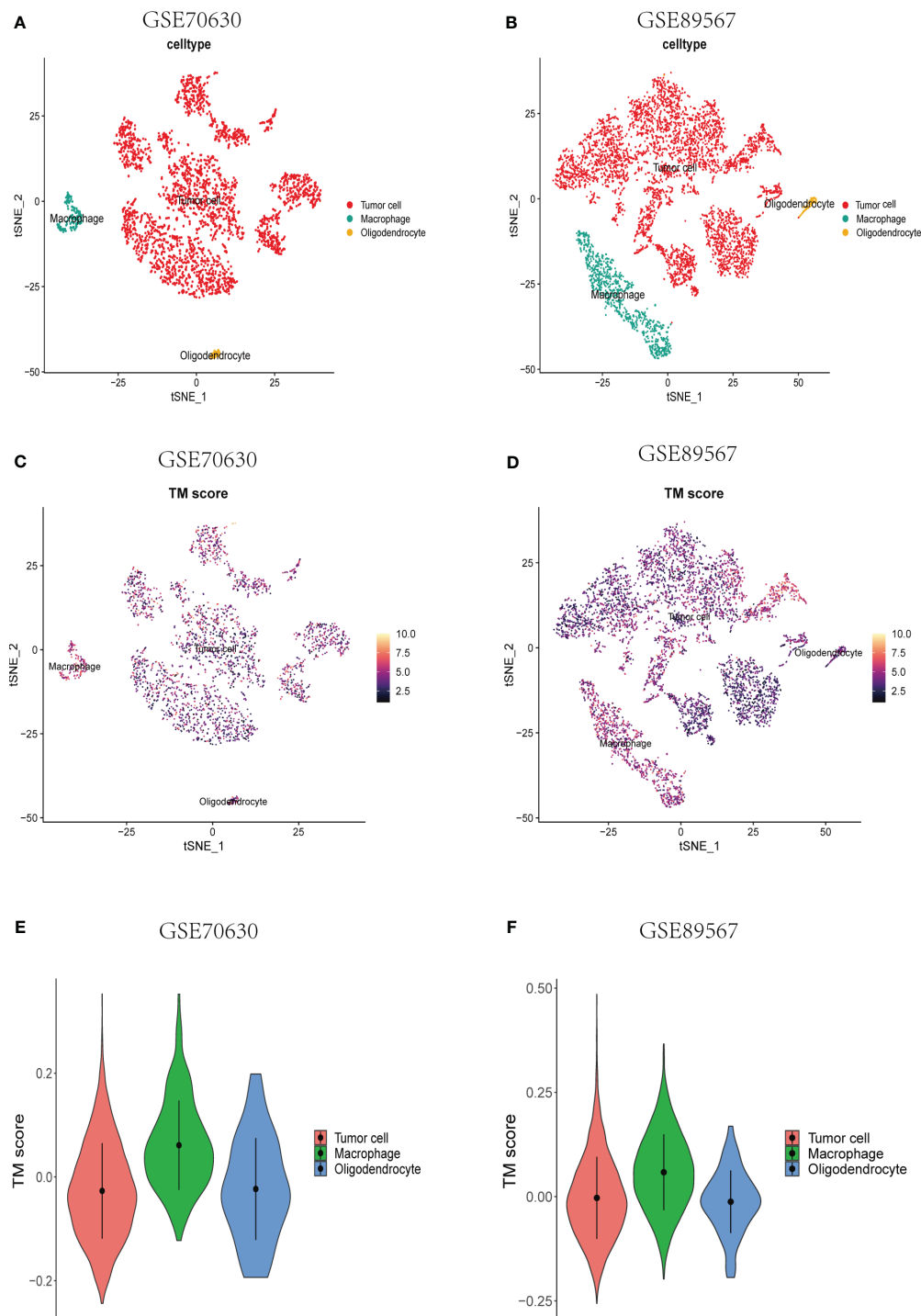


FIGURE 4 Single-cell analyses of the correlation between TM score and various types of cells at the single-cell level. **(A, B)** A t-SNE plot consisting of all cells from the different data sets. Annotation of the cells was done using the established gene markers. **(C, D)** A t-SNE plot depicting all single cells, each colored according to the TM score from the two datasets, respectively. **(E, F)** TM score comparisons across tumor cells, macrophages, and oligodendrocytes.

subgroup were the yellow and pink modules (Figure 7D). Similarly, we selected the brown module as the representative key module for the TM_L+TME_H subgroup. Subsequently, functional enrichment analysis was conducted using Metascape, applying a

cutoff of min overlap = 3, p-value cutoff = 0.01, and min enrichment = 1.5. This analysis revealed 20 enriched pathways in the TM_H+TME_L and TM_L+TME_H subgroups (Figures 7E, F). The TM_H+TME_L subgroup was primarily associated with the cell



FIGURE 5 Telomere related genes expression in LGG TME-associated cells. (A) GSE131928 annotation of all cell types and percentage of each cell type. (B) Percentages of 17 telomere related genes in LGG.

cycle and DNA metabolic process, while the TM_L+TME_H subgroup exhibited a stronger association with the neuronal system and modulation of chemical synaptic transmission. For the identification of protein complexes, we utilized MCODE with the following criteria: physical score > 0.132, min network size = 3, max network size = 500, and databases as physical core (Supplementary Figures S2D–G).

The ROC analysis demonstrated that the TM-TME classifier effectively predicted overall survival (OS) at 3, 5, and 7 years,

yielding area under the curve (AUC) values of 0.813, 0.795, and 0.815, respectively (Figure 8E). To investigate the comprehensive prognostic significance of the TM-TME classifier, we performed univariate and multivariate Cox regression analyses in the TCGA LGG cohort. These analyses revealed that the TM-TME classifier served as an independent unfavorable prognostic factor (Figures 8A, B). Additionally, this finding was validated in the CGGA LGG cohort (Figures 8C, D). Furthermore, we generated KM OS curves for the TM-TME classifier across various TCGA LGG clinical subtypes

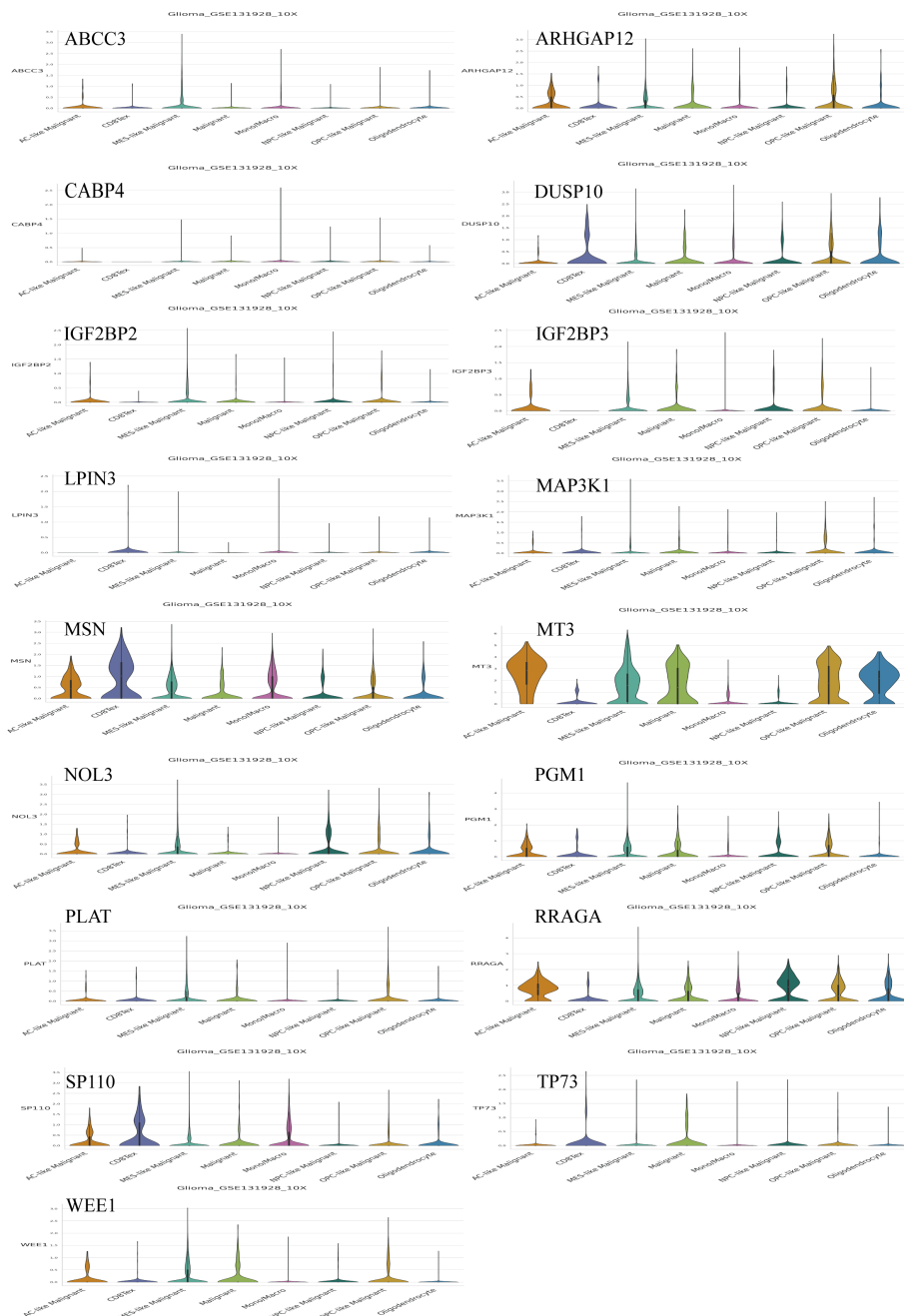


FIGURE 6 Expressions of 17 telomere related genes in LGG.

(Supplementary Figure S3). These curves demonstrated the effective prognostic prediction of the TM-TME classifier in the majority of TCGA LGG clinical subtypes. Therefore, the TM-TME classifier exhibits broad applicability for predicting prognosis in LGG.

3.6 Distinct SM landscapes across TM-TME subgroups

Immune checkpoint therapy confers long-term clinical benefits to patients in the field of oncology (44). Consequently, we investigated the

expression profiles of crucial checkpoint genes and major histocompatibility complex (MHC) across distinct subgroups within the TM-TME paradigm. Notably, within the TCGA LGG cohort, significant variations in expression were observed for most checkpoint genes and MHC components (Figures 9A, B). Interestingly, the TM_H +TME_L subgroup exhibited elevated expression levels of MHCs and a majority of checkpoint genes, including *BTN2A1*, *BTN2A2*, *CD274*, *CD276*, *CD86*, *CTLA4*, among others.

The occurrence and accumulation of somatic mutations (SMs) span an individual’s lifetime, with a proposed theory suggesting that the progressive accumulation of genetic mutations contributes

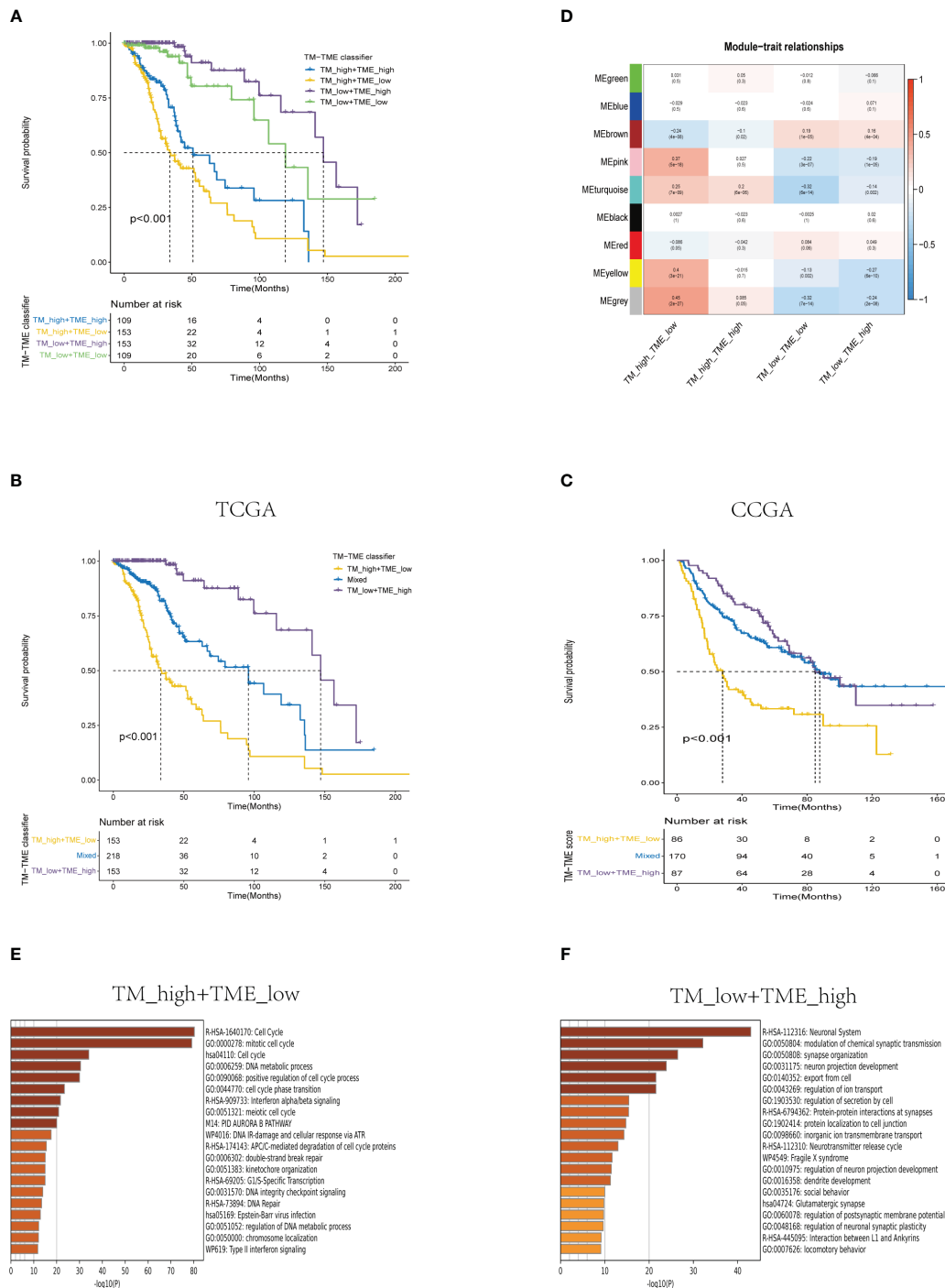


FIGURE 7 Analysis of the prognostic significance and enrichment of the TM-TME classifier. **(A)** Kaplan-Meier overall survival curves of the TCGA LGG tumors classified into four diverse subgroups as per the TM-TME classifier. **(B, C)** KM-OS curves of the training dataset (TCGA LGG cohort) and validation set (CCGA LGG cohort) based on the TM-TME classifier. **(D)** A heatmap depicting the association between the subgroups of the TM-TME classifier and the module eigengenes. The Pearson correlation coefficients as well as the P values are displayed in each cell. **(E, F)** Top 20 pathways enriched in TM_H+TME_L subgroup and TM_L+TME_H subgroup, respectively.

to the onset and progression of cancer (45). In addition, we explored the landscape of SMs across different subgroups within the TM-TME context. To illustrate this, **Figures 9C, D** presents a waterfall diagram showcasing the top 20 genes with the highest mutation

frequencies in the TM_L+TME_H and TM_H+TME_L subgroups. In comparison to the TM_H+TME_L subgroup, the TM_L+TME_H subgroup exhibited a higher incidence of both gene mutations and mutations occurring in patients. The mutation rate

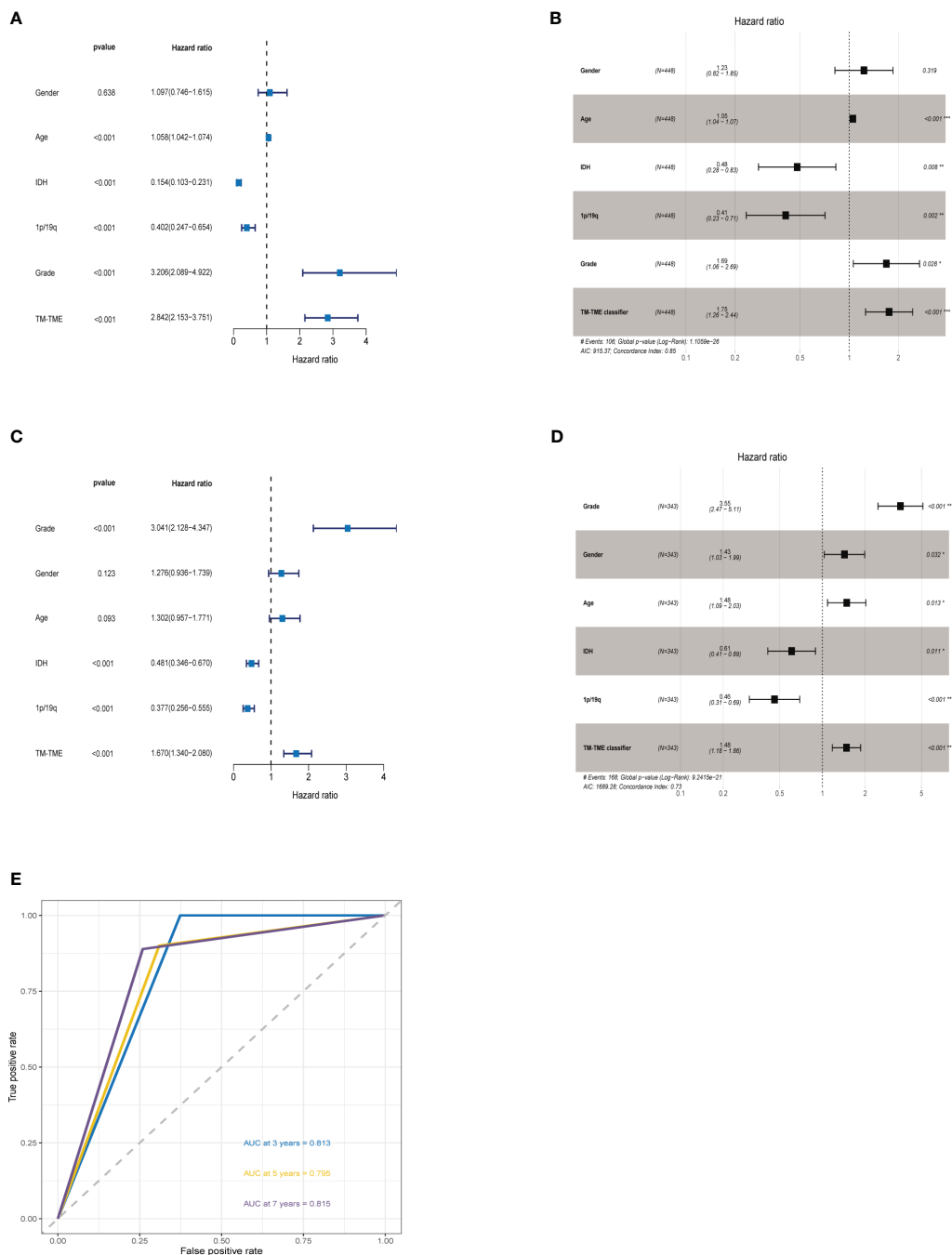


FIGURE 8 TM-TME classifier relationships with clinical characteristics in LGG. **(A, B)** Univariate and Multivariate Cox analyses of clinical characteristics and TM-TME classifier in TCGA LGG cohort. **(C, D)** Univariate and Multivariate Cox analysis of clinical characteristics and TM-TME classifier in CGGA LGG cohort. **(E)** OS-ROC curves over 3, 5, and 7 years on the basis of the TM-TME classifier in the TCGA LGG cohort.

in the TM_L+TME_H subgroup reached 99.32%, whereas the TM_H+TME_L subgroup had a mutation rate of 92.81%. Furthermore, distinct differences between the subgroups were observed in terms of higher frequencies of IDH1 mutations (94% in the TM_L+TME_H subgroup and 52% in the TM_H+TME_L subgroup), TP53 mutations (56% in the TM_L+TME_H subgroup

and 37% in the TM_H+TME_L subgroup), and ATRX mutations (47% in the TM_L+TME_H subgroup and 21% in the TM_H+TME_L subgroup). Integrating the TM-TME classifier with tumor mutational burden (TMB) using the median TMB value in patients from the TCGA LGG cohort, we discovered a negative association between TMB and patients' prognoses in the dataset (Figure 9E).

3.7 TM-TME classifier guided LGG therapy approaches

Immunotherapy-based strategies currently dominate as the prevailing therapeutic approaches for cancer. We employed TIDE to predict the response to immunotherapy in various subgroups of

the tumor microenvironment (TM-TME). Notably, the responder group exhibited lower TM and TME scores in contrast to the non-responder group (Figures 9F, G). In specific subgroups, namely TM_L+TME_H, Mixed, and TM_H+TME_L, the response rates to immunotherapy were 59%, 44%, and 19%, respectively (Figure 9H). Of particular interest, the TM_L+TME_H subgroup demonstrated

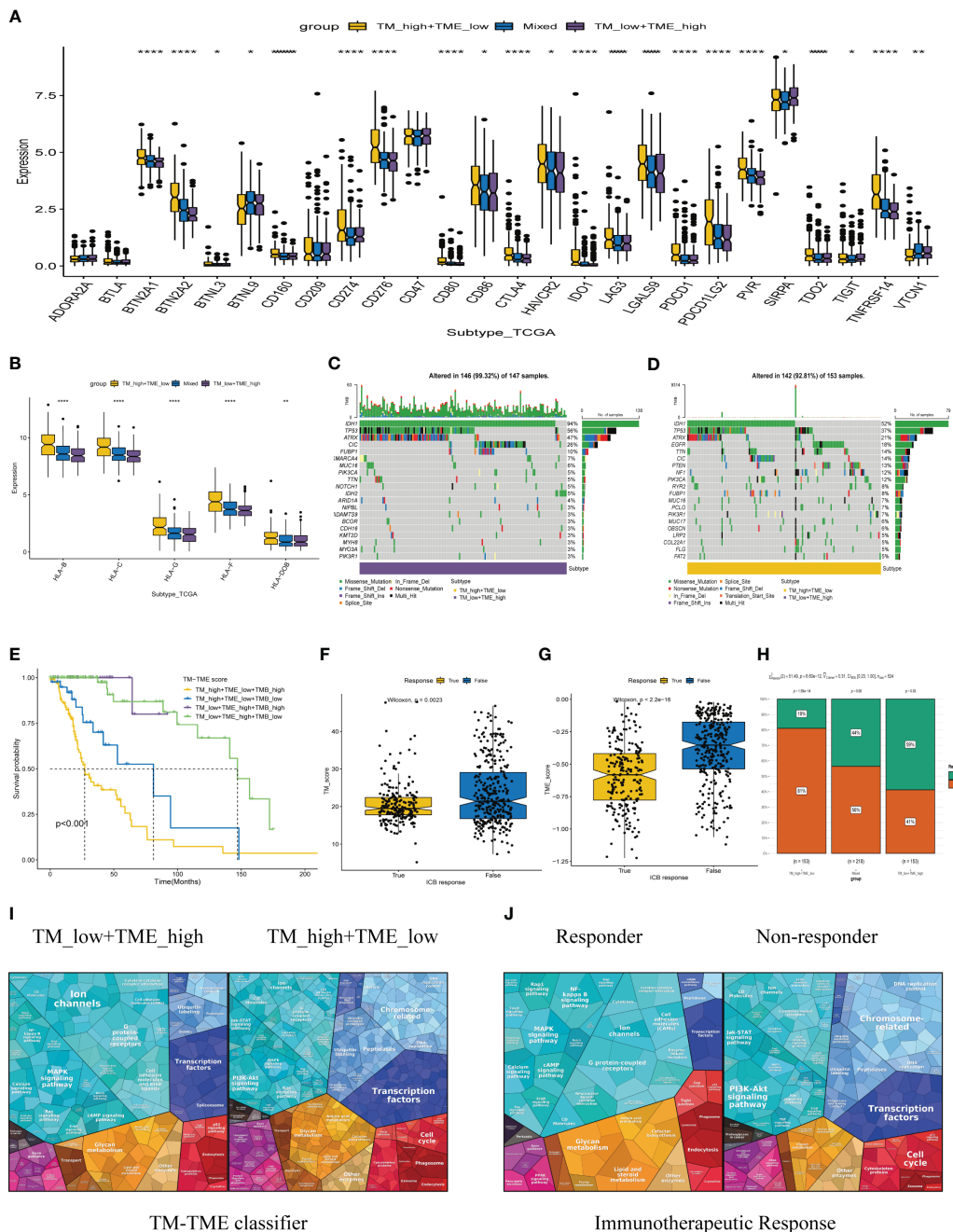


FIGURE 9
 The TCGA-LGG cohort-related TM-TME classifier shows associations with immune checkpoints and somatic mutation. **(A)** Immune checkpoint genes with differential expression across various TM-TME classifier subgroups. **(B)** The differential expression levels of major histocompatibility complex (MHC) among TM-TME classifier subgroups. **(C, D)** Differences in mutations between the TM_H+TME_L subgroup and the TM_L+TME_H subgroup (the top 20 mutated genes). **(E)** KM-OS curves among four groups divided by TMB and TM-TME classifier. * $p < 0.05$, ** $p < 0.01$, *** $p < 0.0001$. **(F, G)** The TM and TME scores have different distributions among those who respond to immunotherapy and those who do not respond. **(H)** Comparison of immunotherapy responses across different TM-TME classifier groups in TCGA LGG cohort. **(I, J)** Functional analysis proteomaps of immunotherapy responders and non-responders in TM_H+TME_L, TM_L+TME_H subgroups. Polygons represent each KEGG pathway, with their sizes reflecting the protein ratio in each.

a significantly higher likelihood of benefiting from immunotherapy compared to the other two subgroups. To visually depict and differentiate the underlying processes among LGG patients in distinct groups, proteomaps were utilized (Figures 9I, J). Notably, the proteomaps of the TM_L+TME_H subgroup and responder groups exhibited a remarkably high level of similarity, while a similar observation was made between the TM_H+TME_L subgroup and non-responder groups. This indicates the effective characterization of the TME in LGG patients and the ability of the TM-TME classifier to predict the outcome of immunotherapy.

3.8 The expression levels of 17 prognostic risk genes

Using our bioinformatics analysis findings as a basis, we conducted additional investigations into the expression patterns of the 18 prognostic risk genes within five LGG tissues as well as their corresponding peritumoral tissues among patients. Employing qRT-PCR at the transcriptional level, we observed noteworthy disparities in the expression levels of four genes (ARHGAP, MAP3K1, SP110, and WEE1) between LGG and peritumoral tissues. However, no significant differences were detected in the expression levels of the remaining genes. Notably, GATA5 was undetectable in both LGG and peritumoral tissues as determined by qRT-PCR analysis (Figure 10).

3.9 The expression levels of WEE1 in LGG

We conducted a random selection of a specific gene, WEE1, to investigate its protein expression patterns. Our analysis utilizing Western blotting (WB), immunohistochemistry (IHC), and immunofluorescence staining revealed a substantial elevation of WEE1 levels within the tumor tissues, in comparison to the corresponding adjacent tumor tissues. These findings strongly suggest that WEE1 holds great promise as a potential therapeutic target for glioma treatment (Figures 11, 12).

4 Discussion

Telomeres have a crucial impact on the advancement of lower-grade glioma and the modulation of the tumor microenvironment (TME) (46). Limited investigations have explored the joint utilization of telomere and TME signatures to forecast prognosis and treatment response. The development of multi-omics has greatly improved the diagnostic and predictive accuracy of diseases (47, 48). In this novel investigation, we present the inaugural integration of telomere and TME signatures, resulting in the development of a TM-TME classifier capable of enhancing clinical categorization and refining treatment strategies.

In our study, we established the TM score utilizing the 18 genes associated with telomeres. Previous investigations have indicated the upregulation of ABCC3 (ATP binding cassette subfamily C member 3) in glioma patients (49). The hypomethylation of ABCC3 has been observed in LGG patients with epilepsy, which is associated with unfavorable prognoses (50). Furthermore, the methylation of GATA5 (GATA binding protein 5) has been identified in 27.8% of glioblastoma patients and is strongly correlated with poor outcomes in primary glioblastoma cases (51). Activation of the PI3K/Akt signaling pathway by IGF2BP2 (also known as Imp2, Insulin-like growth factor 2 mRNA-binding protein 2) promotes glioma progression, while its inhibition sensitizes glioma cells to temozolomide treatment (52). Glioma cell proliferation, invasion, and tumor propagation have been found to be facilitated by IGF2BP3, as observed by Jin et al. (53). Extensive research has shown that MAP3K1 plays a crucial role in cell migration, growth, and apoptosis, and its dysregulation is closely associated with adverse outcomes in various malignancies, including glioma (54–57). Some genes, such as CABP4, DUSP10, LPIN3, were reported for the first time to be associated with glioma.

The immune system plays a crucial role in cancer development and the advancement of immunotherapy (58). Extensive research is currently being conducted on exosome-based immunotherapy (59, 60). It is noteworthy that metabolic molecules exert a substantial influence on the immune environment, thereby impacting disease progression (61–63). Moreover, the equilibrium of cytokines holds significant sway over the advancement of diseases (64). To better understand the role of immune cells in lower-grade glioma, subsequently, we developed the TME score based on five TME cells: eosinophils, activated mast cells, monocytes, plasma cells, and activated NK cells. These cells are all associated with a favorable prognosis in LGG patients. Eosinophils, derived from myeloid progenitors, have been found to correlate with improved prognoses in several solid tumors, including glioma, colon cancer, and lung cancer, due to their infiltration and degranulation (65–67). Mast cells suppress the signal transducer and activator of transcription 3 (STAT3) pathway by downregulating glycogen synthase kinase 3 β (GSK3 β), thereby diminishing the proliferation, migration, and invasion of glioma cells (68). Monocytes are found in the spleen, blood, and bone marrow (69). They encompass three subtypes: monocytes, repolarized monocytes, and monocytes that differentiate into macrophages (70). Wang et al. observed a decrease in invasive monocyte counts and a subtype-dependent increase in macrophage/microglia numbers during glioma recurrence, as determined by a gene signature associated with the TME (71). The expression of B cell and plasma cell signature genes has been positively correlated with overall survival (OS) in patients with pancreatic cancer, melanoma, and lung adenocarcinoma. However, elevated expression levels of these genes have been associated with poorer clinical outcomes in patients with glioblastoma and clear cell renal cell carcinoma (72–74).

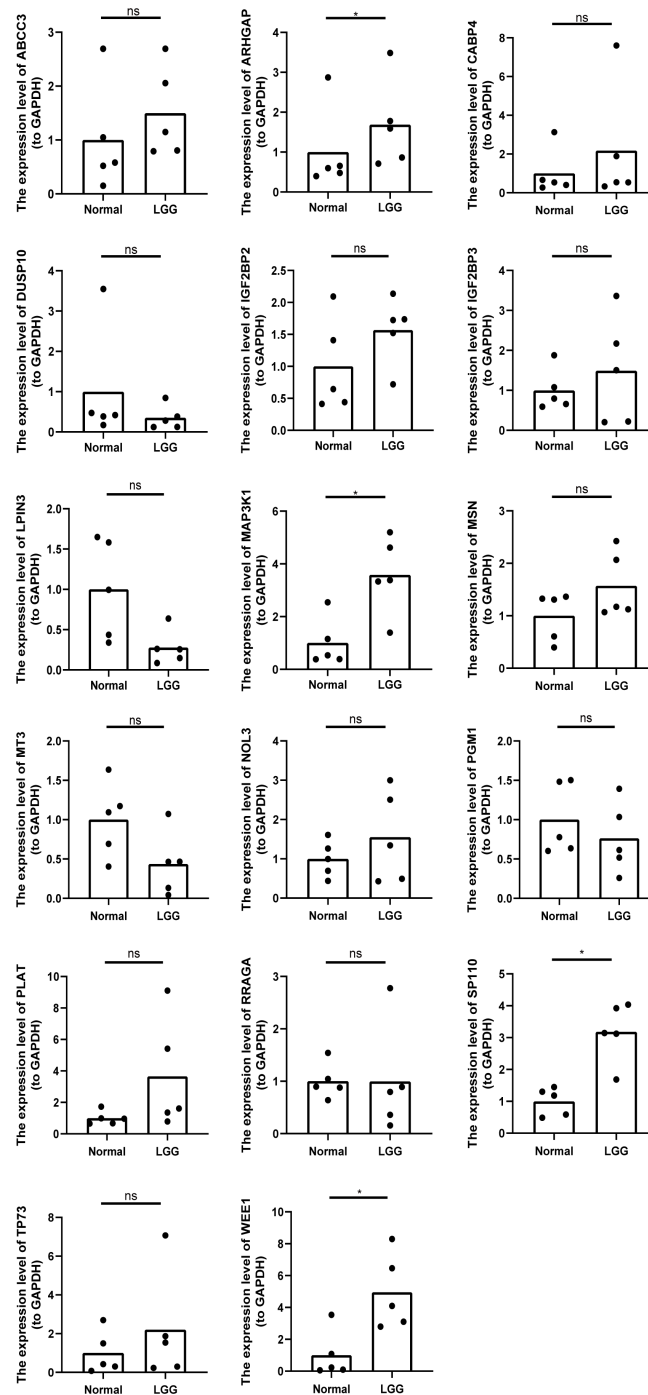


FIGURE 10 The relative expression levels of 17 genes (except GATA5) in five LGG tissues and the corresponding peritumoral tissues of patients. * $p < 0.05$, ns represents no significant difference.

The TM-TME classifier was established based on the TM and TME scores. Analysis using Gene Ontology (GO) indicated that the TM_L+TME_H subgroup is associated with neuronal system function and the modulation of chemical synaptic transmission. Notably, studies have demonstrated that gliomas can perturb neuronal plasticity and development within the TME, leading to

aberrant neuronal connections with tumor cells through neuronal glioma synapses (75, 76). On the other hand, the TM_H+TME_L subgroup exhibits a stronger correlation with cell cycle regulation and DNA metabolic processes. Previous research by Roth et al. has highlighted the role of glycosylation, lipid metabolism, and carbohydrate metabolism in promoting tumor malignancy,

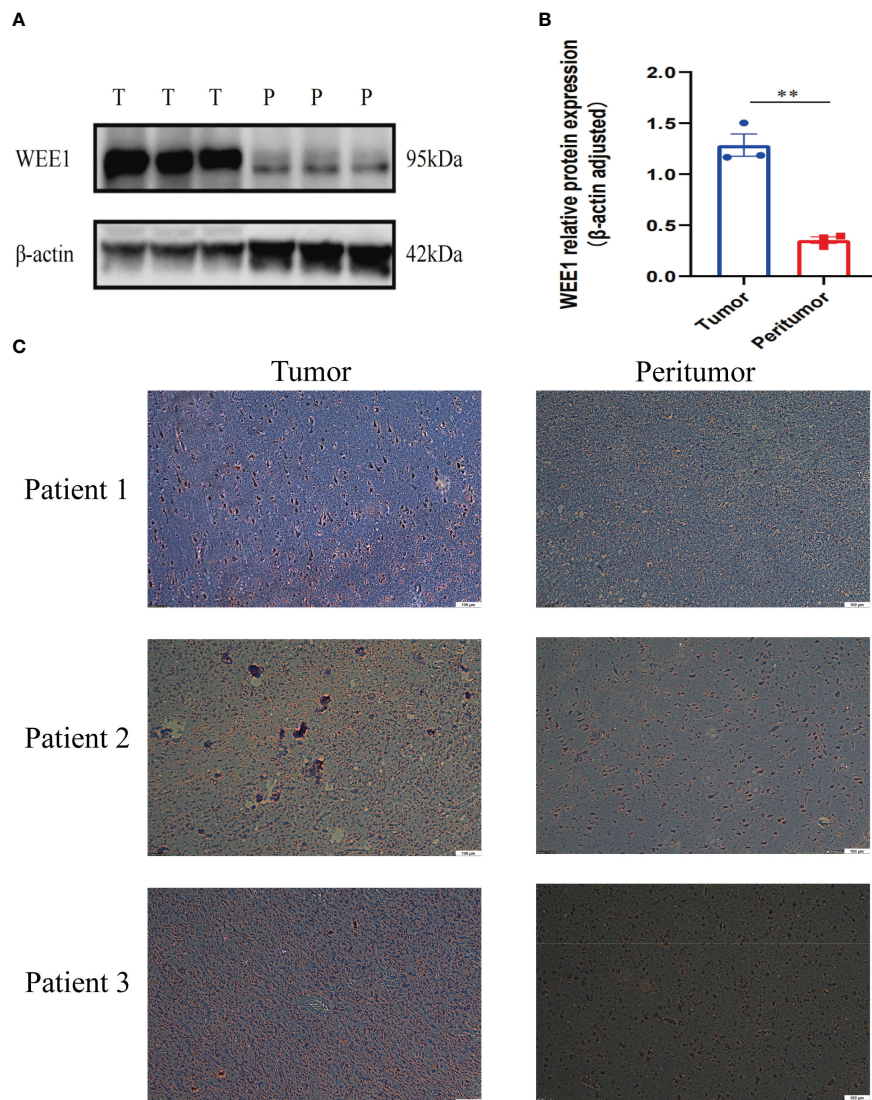


FIGURE 11

(A) WB for WEE1 in tumor tissues and peritumor tissues from one patient. (B) The expression level of WEE1 in tumor tissue and peritumor tissue. (C) IHC for WEE1 in paired tumor tissues and peritumor tissue from three patients. ** $p < 0.01$.

thereby identifying novel therapeutic targets (77). Consistently, our findings reveal a poorer prognosis in the TM_H+TME_L subgroup.

Interestingly, patients assigned to the TM_L+TME_H subgroup displayed the most favorable prognosis, which was positively associated with higher tumor mutational burden (TMB). TMB has emerged as a potential biomarker for predicting the efficacy of immune checkpoint blockade (ICB) therapy. Hence, the TM_L+TME_H subgroup exhibits a higher rate of immune response to treatment. In contrast, the TM_H+TME_L subgroup exhibited the poorest prognosis, accompanied by the lowest immune response rate. These results are in line with previous perspectives on the relationship between TMB and immunotherapy (78).

In brief, we have delineated the combined molecular profiles of telomeres and immune cells in the tumor microenvironment (TME). This comprehensive analysis provides a fresh perspective on the classification of low-grade gliomas (LGGs) and offers accurate prognostic predictions as well as insights into the effectiveness of immune-based therapies. Nonetheless, it is important to acknowledge the limitations of our study. Firstly, the sample size utilized in our investigation was relatively small, which may impact the generalizability of our findings. Secondly, the inclusion of 18 telomere-associated genes in our analysis poses a significant challenge in terms of experimental validation. Besides, the migratory capacity and drug resistance of tumor cells are closely associated with adverse prognosis and recurrence, thus

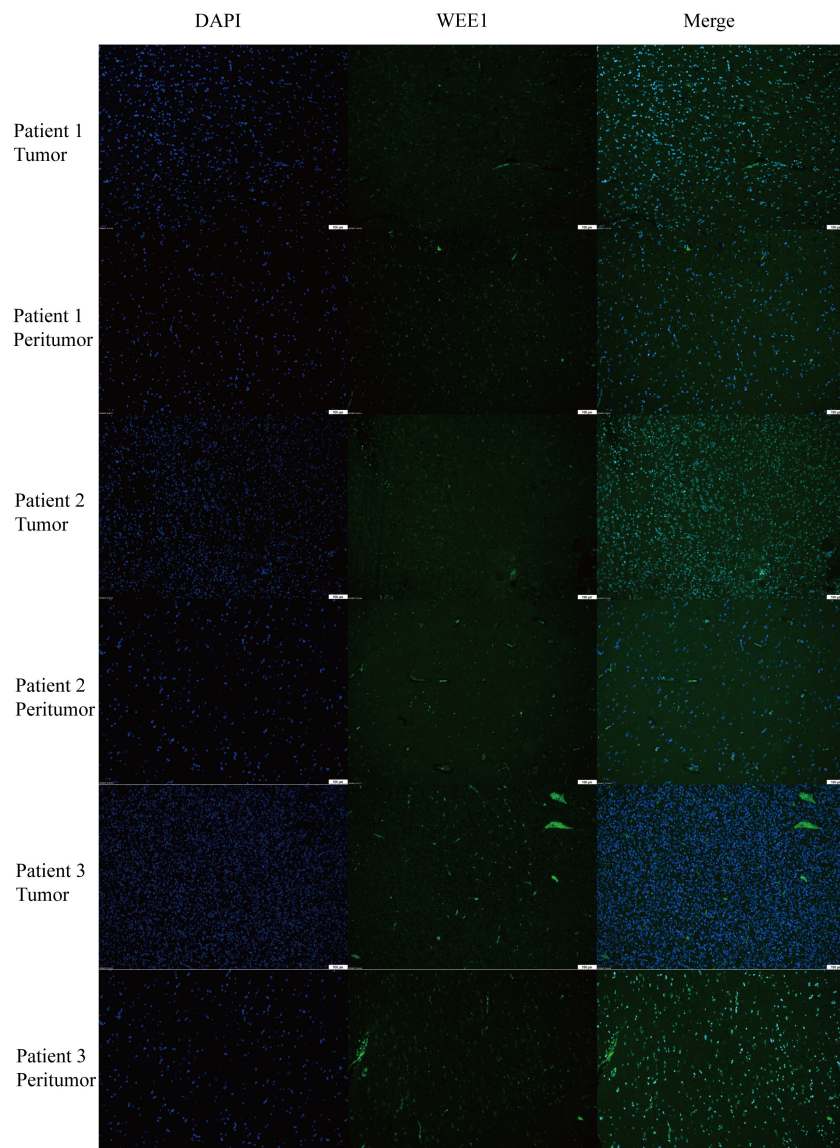


FIGURE 12
Immunofluorescence staining for WEE1 in paired tumor tissues and peritumoral tissue from three patients.

necessitating further experimental elucidation of underlying mechanisms (79, 80). Lastly, the absence of an LGG-specific dataset for assessing the performance of our classifier, despite its validation in the TCGA and CCGA cohorts, is a notable constraint.

Data availability statement

The datasets presented in this study can be found in online repositories. The names of the repository/repositories and accession number(s) can be found within the article/[Supplementary Material](#).

Ethics statement

The studies involving human participants were reviewed and approved by the Ethical Review Committee of Beijing Tiantan

Hospital. The patients/participants provided their written informed consent to participate in this study.

Author contributions

XH and JG conceived the study and collected and analyzed the data. XH wrote the manuscript. JG, YZ, LA provided technical guidance and experimental guidance. XH, ZY, KF, XG, BH, XL, YO, BC contributed to data collection, analysis and interpretation, and manuscript writing. All authors contributed to the article and approved the submitted version.

Funding

This research was funded by the National Natural Science Foundation of China (No.81870834 and No.62276027).

Acknowledgments

We sincerely thank YZ and BC from Beijing Institute of Brain Disorders for experimental guidance.

Conflict of interest

The authors declare that the research was conducted in the absence of any commercial or financial relationships that could be construed as a potential conflict of interest.

Publisher's note

All claims expressed in this article are solely those of the authors and do not necessarily represent those of their affiliated organizations, or those of the publisher, the editors and the reviewers. Any product that may be evaluated in this article, or claim that may be made by its manufacturer, is not guaranteed or endorsed by the publisher.

References

- Louis DN. Molecular pathology of Malignant gliomas. *Annu Rev Pathol* (2006) 1:97–117. doi: 10.1146/annurev.pathol.1.110304.100043
- Louis DN, Perry A, Reifenberger G, von Deimling A, Figarella-Branger D, Cavenee WK, et al. The 2016 World Health Organization classification of tumors of the central nervous system: a summary. *Acta Neuropathol* (2016) 131:803–20. doi: 10.1007/s00401-016-1545-1
- Jiang T, Mao Y, Ma W, Mao Q, You Y, Yang X, et al. CGCG clinical practice guidelines for the management of adult diffuse gliomas. *Cancer Lett* (2016) 375:263–73. doi: 10.1016/j.canlet.2016.01.024
- Adkins K, Crago E, Kuo CW, Horowitz M, Sherwood P. Correlation between ED symptoms and clinical outcomes in the patient with aneurysmal subarachnoid hemorrhage. *J Emerg Nurs* (2012) 38:226–33. doi: 10.1016/j.jen.2010.09.003
- Cairncross G, Wang M, Shaw E, Jenkins R, Brachman D, Buckner J, et al. Phase III trial of chemoradiotherapy for anaplastic oligodendroglioma: long-term results of RTOG 9402. *J Clin Oncol* (2013) 31:337–43. doi: 10.1200/JCO.2012.43.2674
- Shay JW, Wright WE. Telomeres and telomerase: three decades of progress. *Nat Rev Genet* (2019) 20:299–309. doi: 10.1038/s41576-019-0099-1
- Savage SA. Beginning at the ends: telomeres and human disease. *F1000Res* (2018) 7. doi: 10.12688/f1000research.14068.1
- Haycock PC, Burgess S, Nounu A, Zheng J, Okoli GN, Bowden J, et al. Association between telomere length and risk of cancer and non-neoplastic diseases: A mendelian randomization study. *JAMA Oncol* (2017) 3:636–51. doi: 10.1001/jamaoncol.2017.2316
- Liu N, Guo XH, Liu JP, Cong YS. Role of telomerase in the tumour microenvironment. *Clin Exp Pharmacol Physiol* (2020) 47:357–64. doi: 10.1111/1440-1681.13223
- Liu Z, Li Q, Li K, Chen L, Li W, Hou M, et al. Telomerase reverse transcriptase promotes epithelial-mesenchymal transition and stem cell-like traits in cancer cells. *Oncogene* (2013) 32:4203–13. doi: 10.1038/ncr.2012.441
- Liu N, Ding D, Hao W, Yang F, Wu X, Wang M, et al. hTERT promotes tumor angiogenesis by activating VEGF via interactions with the Sp1 transcription factor. *Nucleic Acids Res* (2016) 44:8693–703. doi: 10.1093/nar/gkw549
- Terah K, Yilmazer A. New surprises from an old favourite: The emergence of telomerase as a key player in the regulation of cancer stemness. *Biochimie* (2016) 121:170–8. doi: 10.1016/j.biochi.2015.12.001
- Labussière M, Di Stefano AL, Gleize V, Boisselier B, Giry M, Mangesius S, et al. TERT promoter mutations in gliomas, genetic associations and clinico-pathological correlations. *Br J Cancer* (2014) 111:2024–32. doi: 10.1038/bjc.2014.538

Supplementary material

The Supplementary Material for this article can be found online at: <https://www.frontiersin.org/articles/10.3389/fimmu.2023.1220100/full#supplementary-material>

SUPPLEMENTARY FIGURE 1

The expression analysis of marker genes using single cell analysis. (A, B) t-SNE plot of cells from two datasets, respectively, with each color and number coded to indicate the associated cell types. (C, D) DotPlots show the expression levels of marker genes in each cluster of two datasets, respectively.

SUPPLEMENTARY FIGURE 2

WGCNA analysis and construction of interactive network. GO enrichment analysis was applied to each MCODE network. The same color nodes represent an interactive network and perform similar biological functions. (A) Clustering of sample data to detect outliers. (cutHeight =160) (B) Analysis of the scale-free fit index (left) and the mean connectivity (right) for various soft-thresholding power value. (C) Dendrogram of 5000 selected genes clustered based on a dissimilarity measure (1-TOM) together with assigned module colors. (D) Seven MCODE components were constructed with the screened hub genes in TM_high+TME_low subgroup. (E) Each interactive network with different colors own different score values in TM_high+TME_low subgroup. (F) Eleven MCODE components were constructed with the screened hub genes in TM_low+TME_high subgroup. (G) Each interactive network with different colors owns different score values in TM_low+TME_high subgroup.

SUPPLEMENTARY FIGURE 3

Kaplan-Meier overall survival curves of TM-TME classifier in diverse LGG clinical subtypes in TCGA LGG cohort (A–J).

- Pekmezci M, Rice T, Molinaro AM, Walsh KM, Decker PA, Hansen H, et al. Adult infiltrating gliomas with WHO 2016 integrated diagnosis: additional prognostic roles of ATRX and TERT. *Acta Neuropathol* (2017) 133:1001–16. doi: 10.1007/s00401-017-1690-1
- Zhao Z, Zhang KN, Wang Q, Li G, Zeng F, Zhang Y, et al. Chinese glioma genome atlas (CGGA): A comprehensive resource with functional genomic data from Chinese glioma patients. *Genomics Proteomics Bioinf* (2021) 19:1–12. doi: 10.1016/j.gpb.2020.10.005
- Tirosh I, Venteicher AS, Hebert C, Escalante LE, Patel AP, Yizhak K, et al. Single-cell RNA-seq supports a developmental hierarchy in human oligodendroglioma. *Nature* (2016) 539:309–13. doi: 10.1038/nature20123
- Venteicher AS, Tirosh I, Hebert C, Yizhak K, Neftci C, Filbin MG, et al. Decoupling genetics, lineages, and microenvironment in IDH-mutant gliomas by single-cell RNA-seq. *Science* (2017) 355. doi: 10.1126/science.aai8478
- Braun DM, Chung I, Kepper N, Deeg KI, Rippe K. TelNet - a database for human and yeast genes involved in telomere maintenance. *BMC Genet* (2018) 19:32. doi: 10.1186/s12863-018-0617-8
- Zhang X, Zhuge J, Liu J, Xia Z, Wang H, Gao Q, et al. Prognostic signatures of sphingolipids: Understanding the immune landscape and predictive role in immunotherapy response and outcomes of hepatocellular carcinoma. *Front Immunol* (2023) 14:1153423. doi: 10.3389/fimmu.2023.1153423
- Wang J, Li Y, Fu W, Zhang Y, Jiang J, Zhang Y, et al. Prognostic nomogram based on immune scores for breast cancer patients. *Cancer Med* (2019) 8:5214–22. doi: 10.1002/cam4.2428
- Chi H, Xie X, Yan Y, Peng G, Strohmeyer DF, Lai G, et al. Natural killer cell-related prognosis signature characterizes immune landscape and predicts prognosis of HNSCC. *Front Immunol* (2022) 13:1018685. doi: 10.3389/fimmu.2022.1018685
- Newman AM, Liu CL, Green MR, Gentles AJ, Feng W, Xu Y, et al. Robust enumeration of cell subsets from tissue expression profiles. *Nat Methods* (2015) 12:453–7. doi: 10.1038/nmeth.3337
- Chi H, Yang J, Peng G, Zhang J, Song G, Xie X, et al. Circadian rhythm-related genes index: A predictor for HNSCC prognosis, immunotherapy efficacy, and chemosensitivity. *Front Immunol* (2023) 14:1091218. doi: 10.3389/fimmu.2023.1091218
- Chi H, Jiang P, Xu K, Zhao Y, Song B, Peng G, et al. A novel anoikis-related gene signature predicts prognosis in patients with head and neck squamous cell carcinoma and reveals immune infiltration. *Front Genet* (2022) 13:984273. doi: 10.3389/fgene.2022.984273

25. Ren Q, Zhang P, Lin H, Feng Y, Chi H, Zhang X, et al. A novel signature predicts prognosis and immunotherapy in lung adenocarcinoma based on cancer-associated fibroblasts. *Front Immunol* (2023) 14:1201573. doi: 10.3389/fimmu.2023.1201573
26. Blanche P, Dartigues JF, Jacqmin-Gadda H. Estimating and comparing time-dependent areas under receiver operating characteristic curves for censored event times with competing risks. *Stat Med* (2013) 32:5381–97. doi: 10.1002/sim.5958
27. Wang X, Zhao Y, Strohmmer DF, Yang W, Xia Z, Yu C. The prognostic value of MicroRNAs associated with fatty acid metabolism in head and neck squamous cell carcinoma. *Front Genet* (2022) 13:983672. doi: 10.3389/fgene.2022.983672
28. Satija R, Farrell JA, Gennert D, Schier AF, Regev A. Spatial reconstruction of single-cell gene expression data. *Nat Biotechnol* (2015) 33:495–502. doi: 10.1038/nbt.3192
29. Liu J, Zhang P, Yang F, Jiang K, Sun S, Xia Z, et al. Integrating single-cell analysis and machine learning to create glycosylation-based gene signature for prognostic prediction of uveal melanoma. *Front Endocrinol (Lausanne)* (2023) 14:1163046. doi: 10.3389/fendo.2023.1163046
30. Wu F, Liu YW, Li GZ, Zhai Y, Feng YM, Ma WP, et al. Metabolic expression profiling stratifies diffuse lower-grade glioma into three distinct tumour subtypes. *Br J Cancer* (2021) 125:255–64. doi: 10.1038/s41416-021-01418-6
31. Zhang P, Pei S, Wu L, Xia Z, Wang Q, Huang X, et al. Integrating multiple machine learning methods to construct glutamine metabolism-related signatures in lung adenocarcinoma. *Front Endocrinol (Lausanne)* (2023) 14:1196372. doi: 10.3389/fendo.2023.1196372
32. Sun D, Wang J, Han Y, Dong X, Ge J, Zheng R, et al. TISCH: a comprehensive web resource enabling interactive single-cell transcriptome visualization of tumor microenvironment. *Nucleic Acids Res* (2021) 49:D1420–d1430. doi: 10.1093/nar/gkaa1020
33. Zhao S, Chi H, Yang Q, Chen S, Wu C, Lai G, et al. Identification and validation of neurotrophic factor-related gene signatures in glioblastoma and Parkinson's disease. *Front Immunol* (2023) 14:1090040. doi: 10.3389/fimmu.2023.1090040
34. Langfelder P, Horvath S. WGCNA: an R package for weighted correlation network analysis. *BMC Bioinf* (2008) 9:559. doi: 10.1186/1471-2105-9-559
35. Chi H, Zhao S, Yang J, Gao X, Peng G, Zhang J, et al. T-cell exhaustion signatures characterize the immune landscape and predict HCC prognosis via integrating single-cell RNA-seq and bulk RNA-sequencing. *Front Immunol* (2023) 14:1137025. doi: 10.3389/fimmu.2023.1137025
36. Zhou Y, Zhou B, Pache L, Chang M, Khodabakhshi AH, Tanaseichuk O, et al. Metascape provides a biologist-oriented resource for the analysis of systems-level datasets. *Nat Commun* (2019) 10:1523. doi: 10.1038/s41467-019-09234-6
37. Liebermeister W, Noor E, Flamholz A, Davidi D, Bernhardt J, Milo R. Visual account of protein investment in cellular functions. *Proc Natl Acad Sci USA* (2014) 111:8488–93. doi: 10.1073/pnas.1314810111
38. Mayakonda A, Lin DC, Assenov V, Plass C, Koeffler HP. Maftools: efficient and comprehensive analysis of somatic variants in cancer. *Genome Res* (2018) 28:1747–56. doi: 10.1101/gr.239244.118
39. Chi H, Gao X, Xia Z, Yu W, Yin X, Pan Y, et al. FAM family gene prediction model reveals heterogeneity, stemness and immune microenvironment of UCEC. *Front Mol Biosci* (2023) 10:1200335. doi: 10.3389/fmolb.2023.1200335
40. Fu J, Li K, Zhang W, Wan C, Zhang J, Jiang P, et al. Large-scale public data reuse to model immunotherapy response and resistance. *Genome Med* (2020) 12:21. doi: 10.1186/s13073-020-0721-z
41. Zhao S, Zhang X, Gao F, Chi H, Zhang J, Xia Z, et al. Identification of copper metabolism-related subtypes and establishment of the prognostic model in ovarian cancer. *Front Endocrinol (Lausanne)* (2023) 14:1145797. doi: 10.3389/fendo.2023.1145797
42. Zhang H, Zhai X, Liu Y, Xia Z, Xia T, Du G, et al. NOP2-mediated m5C Modification of c-Myc in an EIF3A-Dependent Manner to Reprogram Glucose Metabolism and Promote Hepatocellular Carcinoma Progression. *Res (Wash D C)* (2023) 6:0184. doi: 10.34133/research.0184
43. Neftel C, Laffy J, Filbin MG, Hara T, Shore ME, Rahme GJ, et al. An integrative model of cellular states, plasticity, and genetics for glioblastoma. *Cell* (2019) 178:835–849.e821. doi: 10.1016/j.cell.2019.06.024
44. Sharma P, Siddiqui BA, Anandhan S, Yadav SS, Subudhi SK, Gao J, et al. The next decade of immune checkpoint therapy. *Cancer Discov* (2021) 11:838–57. doi: 10.1158/2159-8290.CD-20-1680
45. Martincorena I, Campbell PJ. Somatic mutation in cancer and normal cells. *Science* (2015) 349:1483–9. doi: 10.1126/science.aab4082
46. Mao J, Zhang Q, Wang Y, Zhuang Y, Xu L, Ma X, et al. TERT activates endogenous retroviruses to promote an immunosuppressive tumour microenvironment. *EMBO Rep* (2022) 23:e52984. doi: 10.15252/embr.202152984
47. Jin W, Yang Q, Chi H, Wei K, Zhang P, Zhao G, et al. Ensemble deep learning enhanced with self-attention for predicting immunotherapeutic responses to cancers. *Front Immunol* (2022) 13:1025330. doi: 10.3389/fimmu.2022.1025330
48. Wang Q, Li Z, Zhou S, Li Z, Huang X, He Y, et al. NCAPG2 could be an immunological and prognostic biomarker: From pan-cancer analysis to pancreatic cancer validation. *Front Immunol* (2023) 14:1097403. doi: 10.3389/fimmu.2023.1097403
49. Fang DD, Huang W, Cheng G, Liu XN, Liu SM, Hou BS, et al. Clinicopathological and prognostic significance of ABCG3 in human glioma. *J Oncol* (2021) 2011:1827992. doi: 10.1155/2021/1827992
50. Cheng Q, Duan W, He S, Li C, Cao H, Liu K, et al. Multi-omics data integration analysis of an immune-related gene signature in LGG patients with epilepsy. *Front Cell Dev Biol* (2021) 9:686909. doi: 10.3389/fcell.2021.686909
51. Rankeillor KL, Cairns DA, Loughrey C, Short SC, Chumas P, Ismail A, et al. Methylation-specific multiplex ligation-dependent probe amplification identifies promoter methylation events associated with survival in glioblastoma. *J Neurooncol* (2014) 117:243–51. doi: 10.1007/s11060-014-1372-y
52. Mu Q, Wang L, Yu F, Gao H, Lei T, Li P, et al. Imp2 regulates GBM progression by activating IGF2/PI3K/Akt pathway. *Cancer Biol Ther* (2015) 16:623–33. doi: 10.1080/15384047.2015.1019185
53. Jin P, Huang Y, Zhu P, Zou Y, Shao T, Wang O. CircRNA circHIPK3 serves as a prognostic marker to promote glioma progression by regulating miR-654/IGF2BP3 signaling. *Biochem Biophys Res Commun* (2018) 503:1570–4. doi: 10.1016/j.bbrc.2018.07.081
54. Wu L, Yin JH, Guan YY, Liu HL, Shen HL, Wang XJ, et al. A long noncoding RNA MAP3K1-2 promotes proliferation and invasion in gastric cancer. *Oncotargets Ther* (2018) 11:4631–9. doi: 10.2147/OTT.S168819
55. Liu C, Wang S, Zhu S, Wang H, Gu J, Gui Z, et al. MAP3K1-targeting therapeutic artificial miRNA suppresses the growth and invasion of breast cancer. *Vivo vitro. Springerplus* (2016) 5:11. doi: 10.1186/s40064-015-1597-z
56. Chang Y, Yan W, Sun C, Liu Q, Wang J, Wang M. miR-145-5p inhibits epithelial-mesenchymal transition via the JNK signaling pathway by targeting MAP3K1 in non-small cell lung cancer cells. *Oncol Lett* (2017) 14:6923–8. doi: 10.3892/ol.2017.7092
57. Wang J, Zuo J, Wahafu A, Wang MD, Li RC, Xie WF. Combined elevation of TRIB2 and MAP3K1 indicates poor prognosis and chemoresistance to temozolomide in glioblastoma. *CNS Neurosci Ther* (2020) 26:297–308. doi: 10.1111/cns.13197
58. Zhao Y, Wei K, Chi H, Xia Z, Li X. IL-7: A promising adjuvant ensuring effective T cell responses and memory in combination with cancer vaccines? *Front Immunol* (2022) 13:1022808. doi: 10.3389/fimmu.2022.1022808
59. Gong X, Chi H, Strohmmer DF, Teichmann AT, Xia Z, Wang Q. Exosomes: A potential tool for immunotherapy of ovarian cancer. *Front Immunol* (2022) 13:1089410. doi: 10.3389/fimmu.2022.1089410
60. Xiong J, Chi H, Yang G, Zhao S, Zhang J, Tran LJ, et al. Revolutionizing anti-tumor therapy: unleashing the potential of B cell-derived exosomes. *Front Immunol* (2023) 14:1188760. doi: 10.3389/fimmu.2023.1188760
61. Soltani M, Zhao Y, Xia Z, Ganjalikhani Hakemi M, Bazhin AV. The importance of cellular metabolic pathways in pathogenesis and selective treatments of hematological malignancies. *Front Oncol* (2021) 11:767026. doi: 10.3389/fonc.2021.767026
62. Xiao J, Lin H, Liu B, Xia Z, Zhang J, Jin J. Decreased S1P and SPHK2 are involved in pancreatic acinar cell injury. *biomark Med* (2019) 13:627–37. doi: 10.2217/bmm-2018-0404
63. Li Z, Wang Q, Huang X, Yang M, Zhou S, Li Z, et al. Lactate in the tumor microenvironment: A rising star for targeted tumor therapy. *Front Nutr* (2023) 10:1113739. doi: 10.3389/fnut.2023.1113739
64. Xiao J, Huang K, Lin H, Xia Z, Zhang J, Li D, et al. Mogrosin II(E) inhibits digestive enzymes via suppression of interleukin 9/interleukin 9 receptor signalling in acute pancreatitis. *Front Pharmacol* (2020) 11:859. doi: 10.3389/fphar.2020.00859
65. Huang Z, Wu L, Hou Z, Zhang P, Li G, Xie J. Eosinophils and other peripheral blood biomarkers in glioma grading: a preliminary study. *BMC Neurol* (2019) 19:313. doi: 10.1186/s12883-019-1549-2
66. Pretlow TP, Keith EF, Cryar AK, Bartolucci AA, Pitts AM, Pretlow TG2nd, et al. Eosinophil infiltration of human colonic carcinomas as a prognostic indicator. *Cancer Res* (1983) 43:2997–3000.
67. Costello R, O'Callaghan T, Sébahoun G. [Eosinophils and antitumor response]. *Rev Med Interne* (2005) 26:479–84. doi: 10.1016/j.revmed.2005.02.013
68. Attarha S, Roy A, Westermark B, Tchougounova E. Mast cells modulate proliferation, migration and stemness of glioma cells through downregulation of GSK3 β expression and inhibition of STAT3 activation. *Cell Signal* (2017) 37:81–92. doi: 10.1016/j.cellsig.2017.06.004
69. Shi C, Pamer EG. Monocyte recruitment during infection and inflammation. *Nat Rev Immunol* (2011) 11:762–74. doi: 10.1038/nri3070
70. Dal-Secco D, Wang J, Zeng Z, Kolaczowska E, Wong CH, Petri B, et al. A dynamic spectrum of monocytes arising from the *in situ* reprogramming of CCR2+ monocytes at a site of sterile injury. *J Exp Med* (2015) 212:447–56. doi: 10.1084/jem.20141539
71. Wang Q, Hu B, Hu X, Kim H, Squatrito M, Scarpace L, et al. Tumor evolution of glioma-Intrinsic gene expression subtypes associates with immunological changes in the microenvironment. *Cancer Cell* (2017) 32:42–56.e46. doi: 10.1016/j.ccell.2017.06.003
72. Mose LE, Selitsky SR, Bixby LM, Marron DL, Iglesia MD, Serody JS, et al. Assembly-based inference of B-cell receptor repertoires from short read RNA sequencing data with V'DJer. *Bioinformatics* (2016) 32:3729–34. doi: 10.1093/bioinformatics/btw526

73. Bolotin DA, Poslavsky S, Davydov AN, Frenkel FE, Fanchi L, Zolotareva OI, et al. Antigen receptor repertoire profiling from RNA-seq data. *Nat Biotechnol* (2017) 35:908–11. doi: 10.1038/nbt.3979
74. Iglesia MD, Parker JS, Hoadley KA, Serody JS, Perou CM, Vincent BG. Genomic analysis of immune cell infiltrates across 11 tumor types. *J Natl Cancer Inst* (2016) 108. doi: 10.1093/jnci/djw144
75. Venkatesh HS, Johung TB, Caretti V, Noll A, Tang Y, Nagaraja S, et al. Neuronal activity promotes glioma growth through neuroligin-3 secretion. *Cell* (2015) 161:803–16. doi: 10.1016/j.cell.2015.04.012
76. Venkataramani V, Tanev DI, Strahle C, Studier-Fischer A, Fankhauser L, Kessler T, et al. Glutamatergic synaptic input to glioma cells drives brain tumour progression. *Nature* (2019) 573:532–8. doi: 10.1038/s41586-019-1564-x
77. Roth KG, Mambetsariev I, Kulkarni P, Salgia R. The mitochondrion as an emerging therapeutic target in cancer. *Trends Mol Med* (2020) 26:119–34. doi: 10.1016/j.molmed.2019.06.009
78. Cao J, Yang X, Chen S, Wang J, Fan X, Fu S, et al. The predictive efficacy of tumor mutation burden in immunotherapy across multiple cancer types: A meta-analysis and bioinformatics analysis. *Transl Oncol* (2022) 20:101375. doi: 10.1016/j.tranon.2022.101375
79. Li Z, Zhou H, Xia Z, Xia T, Du G, Franziska SD, et al. HMGA1 augments palbociclib efficacy via PI3K/mTOR signaling in intrahepatic cholangiocarcinoma. *Biomark Res* (2023) 11:33. doi: 10.1186/s40364-023-00473-w
80. Zhai X, Xia Z, Du G, Zhang X, Xia T, Ma D, et al. Diseases: LRP1B suppresses HCC progression through the NCSTN/PI3K/AKT signaling axis and affects doxorubicin resistance. *Genes Dis* (2022) 10(5):2082–96. doi: 10.1016/j.gendis.2022.10.021